Top Catal (2008) 48:75–83
DOI 10.1007/s11244-008-9054-7

ORIGINAL PAPER

Solid State and Gas Phase NMR Studies of Immobilized Catalysts and Catalytic Active Nanoparticles

Anna Adamczyk · Yeping Xu · Bernadeta Walaszek · Frank Roelofs · Tal Pery · Karin Pelzer · Karine Philippot · Bruno Chaudret · Hans-Heinrich Limbach · Hergen Breitzke · Gerd Buntkowsky

Published online: 27 March 2008

Abstract In the current study two new classes of stabile, catalytic active nanomaterials are investigated. The first class of nanoparticles consists of an inner metal core. To stabilize their structure the metal core is surrounded by organic ligands or embedded in a polymer. The second class consists of catalysts immobilized on mesoporous silica supports of SBA-3 type silica. Employing a combination of ^{1}H, ^{2}H, ^{13}C and ^{29}Si-solid state NMR spectroscopy the structure of the catalysts is analyzed. As a simple model for the catalytic properties of the particles, the activation of $^{2}H_2$ gas on the surface of the particles is studied. Employing ^{1}H and ^{2}H gas phase NMR the kinetics of simple catalytic model reactions is studied. Employing ^{2}H-NMR solid state NMR spectroscopy, the interaction of the metal surface with the substrate is characterized and kinetic data, which characterize the mobility of the deuterium on the surface, are extracted. For the interpretation of these data, parallel NMR studies of model η^2-bound transition metal complexes are employed, which allow, owing to their simpler geometry and higher sensitivity, a quantitative modeling of the spin dynamics in the NMR experiment.

Keywords Mesoporous silica · Immobilized catalysts · Solid-state NMR · Nano-catalysts · Dihydrogen

A. Adamczyk · F. Roelofs · H. Breitzke · G. Buntkowsky (✉)
Institut für Physikalische Chemie, FSU Jena, Helmholtzweg 4, 07743 Jena, Germany
e-mail: Gerd.Buntkowsky@uni-jena.de

Y. Xu · B. Walaszek · T. Pery · H.-H. Limbach
Institut für Chemie, FU Berlin, Takustr. 3, 14195 Berlin, Germany

K. Pelzer · K. Philippot · B. Chaudret
LCC du CNRS, 205, route de Narbonne, 31077 Toulouse, France

1 Introduction

In recent years, interest has grown in the field of immobilized catalyst, due to their high catalytic efficiency and their application potential in environmentally benign ("green") chemistry. This interest has triggered active research in the synthesis of new materials which are organized on the meso- and nanoscale and several spectroscopic and computational techniques for the characterization of these materials and the kinetic processes on their active surfaces have been developed. Suitable supports for the immobilization are silica materials, due to their reactive surfaces which can serve as a starting point for the immobilization of the catalysts. While conventional silica materials with disordered structures are known for a long time, only several years ago a new class of mesoporous silica materials has become available. Although the silica matrix is disordered on an atomic length scale, they are characterized by a periodic pore structure on the mesoscopic length scale [1–6]. Hence they are referred to as periodic mesoporous silica (PMS). PMS materials consist of pseudo-crystalline powders, where each crystallite constitutes a large number of more or less parallel cylindrical pores. The silica formation takes place in aqueous media using surfactants or amphiphilic block copolymers as structure-directing agents (template). The pore diameters can be adjusted by the templating agents. Typically, they are between 2 and 4 nm in the case of MCM-41 silicas, and between 5 and 12 nm for SBA-silicas [5]. Materials with wider pores (up to 30 nm and more) but non-periodic structures can be synthesized by similar procedures. After silica formation the templating agents are removed by calcination. The high porosity causes a huge inner surface of these materials. Owing to their wide range of pore sizes, they are very versatile molecular sieves. Since the physical properties of their inner surfaces, such as

the surface acidity, can be chemically modified [7, 8], mesoporous silica materials are very promising candidates for catalytic applications. Typical representatives of these materials are MCM-41 and SBA-15. They both exhibit a two-dimensionally hexagonal array of cylindrical pores. Owing to the presence of surface silanol groups at the pore walls, these materials can be chemically tailored to various functions [9]. PMS materials opened up fascinating possibilities for new applications in many fields, including catalysis [10–13], drug delivery or size selective molecular separation [14]. At the same time, these materials are of general interest for fundamental studies of surface–substrate interactions and of dynamics of guest molecules in confinement [15–24].

As catalytic active materials (with high selectivity) we are mainly interested in ruthenium complexes and ruthenium nanoparticles (Fig. 1). For the modeling of their properties we employ stable non-classical transition metal hydrides with η^2-bonded dihydrogen ligands. These compounds may be catalytic precursors or stable models for short-lived intermediate steps in catalysis [25–32]. These transition metal complexes, which have very interesting physical, spectroscopic, and chemical properties, are attracting much experimental and theoretical interest [28, 33–52]. The first of these compounds was a tungsten complex, discovered by Kubas already in 1984 [53, 54]. Later a whole series of different transition metal polyhydrides of the type M-$D_m(D_2)_n$ with hydrogen distances varying between 0.8 and 1.7 Å were synthesized [51, 55–59]. Here, *n* gives the number of hydride and *m* the number of dihydrogen type ligands.

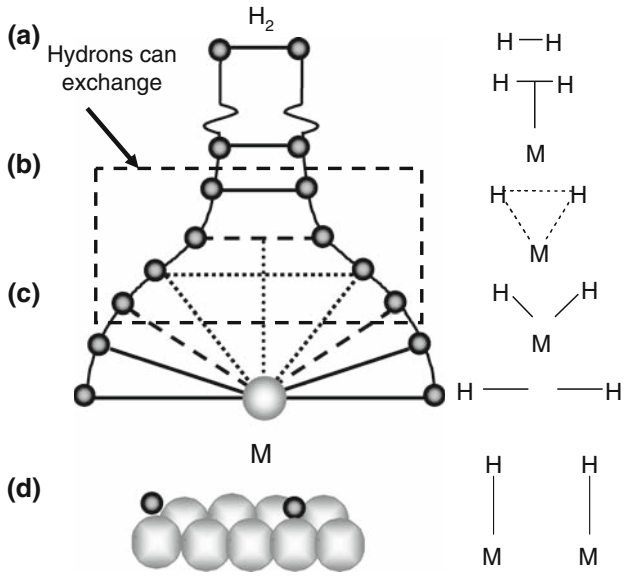

Fig. 1 Schematic hydrogen activation of a hydrogen molecule approaching a metal catalyst or the surface of a catalytic active metal nanoparticle: in the free hydrogen molecule, top, the molecules exist as *para*- and *ortho*-hydrogen spin-isomers. When the molecule approaches the metal, the bond between the two hydrogen atoms is weakened and bonds to the metal are formed. Parallel to this process the two hydrogen atoms form a dihydrogen complex and can perform chemical exchange or tunneling exchange. When the atoms further approach the metal, dihydride complexes are formed, where the barrier of exchange is increased and the hydrogens become immobilized. Finally on metal surfaces the atoms can migrate on the surface

In most transition metal hydrides, dihydride and dihydrogen complexes of the type M-$D_m(D_2)_n$ the hydrogens are relatively weakly bound and exhibit a fairly high mobility. This is in particular true for the dihydrogen ligands which often have only a very weak rotational barrier. Part of this high mobility is due to the exchange symmetry of the two hydrogens in the dihydrogen ligand, which causes tunneling processes at low temperatures which aid in their exchange. A detailed discussion of these tunneling processes and the influence of symmetry effects on hydrogen transfer dynamics is given in Refs. [60, 61]. One example of these complexes are ruthenium complexes of the type L-Ru-$D_m(D_2)_n$, where L stands for different ligands. In particular the two hydrogens in the dihydrogen ligands of a complex can relatively easy perform mutual exchanges. These exchanges correspond physically to a rotational motion of the two hydrogen atoms in the hindering potential of the metal and the other ligands. Owing to these exchange processes the solid state NMR spectra of ruthenium polyhydrogen complexes are fairly complex. In most dihydrogen complexes known so far the rotational barrier is low and this exchange is too fast to be directly observable on the NMR time scale of ^{2}H-NMR spectroscopy and only motional averaged spectra in the fast exchange limit are observed [62]. Moreover, owing to the catalytic activity of the ruthenium, isotope scrambling due to ligand exchange is a common problem in these compounds. For the analysis of their spectra it is necessary to first study simple complexes, which are of pure hydride or dihydrogen type and later transfer this knowledge to more complicated systems.

Similar dynamical processes are found on metal surfaces of ruthenium nanoparticles stabilized in polymer or organic ligand matrices, interacting with hydrogen [63, 64]. However owing to the complex metal surfaces of the nanoparticles and the presence of the organic matrices these systems are far less well defined than the model complexes and more species of deuterium are expected on the surface. The interpretation of their spectra therefore needs studies of the different L-Ru-$D_m(D_2)_n$, complexes which serve as role models for the possible deuterium species on the nanoparticles.

Finally also the flexibility of ligands seems to be an important factor in understanding the catalytic properties of solid or immobilized catalysts. Recently the *ortho–para*

spin conversion and isotope scrambling of dihydrogen in the Vaska's catalyst $Ir(CO)Cl(PPh_3)_2$ in the solid state was studied by NMR [65]. This conversion can occur in two independent ways [66]:

$$H^{\uparrow} - H^{\uparrow} + H^{\uparrow} - H^{\uparrow} \rightleftarrows H^{\uparrow} - H^{\downarrow} + H^{\uparrow} - H^{\downarrow}$$

chemical spin conversion

$$H^{\uparrow} - H^{\uparrow} \rightleftarrows H^{\uparrow} - H^{\downarrow}$$

magnetic spin conversion

They can be distinguished by studying the corresponding isotope scrambling reaction

$$H_2 + D_2 \rightleftarrows 2\,HD,$$

which is only possible for the chemical conversion. In these experiments [65] the efficacy of the catalyst in solution, in phase separated frozen solution and in microcrystalline solids was compared. They delivered the unexpected result that the chemical and not the magnetic spin conversion is the most efficient conversion mechanism at low temperatures and in the solids. This mechanism, however, necessitates the binding of two hydrogen molecules to the catalyst, which should not be possible on a single catalyst molecule. One can only speculate that the flexibility of the ligands or surface defects permit the approach of two dihydrogen molecules bound to different catalyst atoms, which then can cause the isotope scrambling.

The rest of this paper is organized as follows: first we summarize the salient features of the experiments and sample synthesis and preparation, including the grafting of the ruthenium complexes on the silica surfaces. Next we present and discuss experimental results. In the first step we report on the study of two neat complexes. Employing this knowledge we discuss the spectra of ruthenium nanoparticles in the second step. In the last step we then present first results on the immobilization of the ruthenium complexes on silica surfaces.

2 Methods and Materials

2.1 Synthesis of the Mesoporous Silica Support Materials SBA-3

The synthesis of SBA-3 [67] follows the procedure described in Refs. [68, 69]. A mixture of CTMABr (cetyl-methyl-ammonium-bromide) and a non-ionic template, tridecyl-polyoxyethylene(18) ($C_{13}H_{27}$-EO_{18}), with the molar ratio of 1:3 in strong acidic solution is employed. In a typical synthesis, the TEOS was added to the solution of templates and acid (HCl) with a molar ratio of TEOS:template:H_2O:HCl at 1:0.24:28:5. The templates were removed from as-synthesized SBA-3 by calcinations at 550 °C for 16 h, resulting in pure mesoporous silica material.

2.2 Synthesis and Grafting of the Catalysts to the Surface

2.2.1 *Synthesis of Ruthenium Catalyst [$RuHCl(CO)(PPh_3)_3$]*

The synthesis of the catalyst follows the procedure described in Ref. [70]. A solution of $RuCl_3 \cdot 3H_2O$ (2.61 g, 10 mmol) in 2-methoxyethanol (200 mL) and aqueous formaldehyde (200 mL, 40% w/v) were added rapidly and successively to a vigorously stirred boiling solution of TPP (triphenylphosphine) (15.8 g, 60 mL) in the same solvent (300 mL). The mixture was refluxed for 10 min, allowed to cool, filtered, washed with ethanol and hexane successively and dried in vacuum to obtain light brown colored solid.

The structure was confirmed by elementary analysis and ^1H NMR (400 MHz): [ppm] $\delta = 7.68$–7.07 (H_{Ph}), -9.5 (Ru-H).

2.2.2 *Modification of SBA-3 with APTES (3-Aminopropyltriethoxysilane) [71]*

Before modification, the silica material was activated at 423 K in the vacuo for 10 h. Then 3 g of freshly activated silica was refluxed in toluene (50 mL) with APTES (3 g) for 3 h under argon atmosphere. The solid was washed with diethyl ether and Soxhlet extracted with 250 mL dichloromethane yielding covalently anchored APTES moieties.

2.2.3 *Immobilization of $[RuHCl(CO)(PPh_3)_3]$ over NH_2 Modified Silica*

To a suspension of freshly activated NH_2-silica (1 g) in dry toluene (40 mL), a solution of $[RuHCl(CO)(PPh_3)_3]$ (0.1 g) in anhydrous toluene (10 mL) was added and the resulting solution was refluxed for 3 h and the solid was Soxhlet extracted with anhydrous toluene and vacuum dried for 24 h.

2.3 Synthesis of the Nanoparticles

The nanoparticles for this study were prepared as previously reported through hydrogenation of $Ru(C_8H_{10})(C_8H_{12})$ under 3 bar H_2 at room temperature in THF in the presence of 0.2 eq./Ru of hexadecylamine (HDA) and characterized by TEM and WAXS. Details of the synthesis are found in Ref. [72]. The brown colloidal powder thus obtained was used for solid state NMR experiments or redissolved in d_8-THF for solution studies.

2.4 ^{2}H-NMR Powder Spectra

A detailed description of the theory of solid state ^{2}H-NMR is given in the textbooks [73, 74]. Here only some salient facts are briefly summarized.

The leading interaction in ^{2}H-solid state NMR is the quadrupolar interaction. In the usual high field approximation, the first order quadrupolar interaction is characterized by the Hamiltonian

$$\hat{H}_Q = 2\pi\nu_Q(\vartheta,\varphi)\left(\hat{I}_z^2 - \frac{2}{3}\right), \tag{1}$$

where the orientation dependent resonance frequencies ν_Q of the two transitions are given (see Eq. 2.78) in Ref. [74]):

$$\begin{aligned}\nu_Q(\vartheta,\varphi) &= \pm\frac{3}{4}\frac{eQeq}{\hbar}\frac{1}{2}(3\cos^2\vartheta - 1 - \eta\sin^2\vartheta\cos 2\varphi)\\ &= Q_{zz}\frac{1}{2}(3\cos^2\vartheta - 1 - \eta\sin^2\vartheta\cos 2\varphi)\end{aligned} \tag{2}$$

Here η is the asymmetry parameter and Q_{zz} is the principal component of the quadrupolar interaction tensor, i.e., the strength of the quadrupolar interaction. While in single crystals only two lines at $\pm\nu_Q$ are observable, the average over all possible orientations has to be calculated in a polycrystalline powder sample. Due to the axial symmetry of the magnetic field, it is sufficient to integrate over two angles (ϑ, φ). Assuming for simplicity that the transversal relaxation time T_2 is independent on the orientation, the spectra can be calculated as a superposition of the lines with a line shape function $f(\nu, \pm\nu_Q, T_2)$ of the individual crystallites:

$$\begin{aligned}I(\nu) = \int_0^{\pi} d\vartheta\sin(\vartheta)\int_0^{2\pi} d\varphi(f(\nu, -\nu_Q(\vartheta,\varphi), T_2)\\ +f(\nu, +\nu_Q(\vartheta,\varphi), T_2))\end{aligned} \tag{3}$$

Thus for polycrystalline samples a powder average is observed giving rise to the Pake doublet or Pake pattern. For a deuterium atom bound to a carbon atom the most recent value of the quadrupolar coupling constant is found to be $Q_{cc} \cong 170$ kHz [75], corresponding to a strength of the quadrupolar interaction $Q_{zz} = \frac{3}{4}Q_{cc} = 128$ kHz. Owing to fast molecular motions and lattice vibrations, in many solid state NMR experiments a reduced effective value of Q_{cc} is observed, even at low temperatures. Thus in most ^{2}H-NMR experiments Q_{cc} has to be considered as a fitting parameter. In the ^{2}H-NMR study of the iBA molecules, there is a succession of possible intramolecular and molecular rotations of the molecule which cause an averaging of the static quadrupolar interaction, denoted as Q_{zz}^0, to various reduced interactions, denoted as Q_{zz}^n, where n is an index used to distinguish these different averaged tensors.

2.5 Data Evaluation

The ^{2}H-solid-echo-spectra in the fast and slow exchange regime were simulated employing a laboratory written Matlab program. Instead of numerically performing the powder integration, the faster analytical expression of the powder pattern in terms of elliptic integrals [76] was used to calculate the line shape for infinite T_2. Effects of the limited excitation bandwidth were taken into account using the formula given in Ref. [77]. Since the width of the spectra is much larger than the natural line width of the individual crystallites a simple Lorentzian was chosen as line shape function $f(\nu, \pm\nu_Q, T_2)$. The resulting Pake spectra were numerically convoluted with this Lorentzian by Fourier transformation into the time domain, multiplied with a decaying exponential function and transformed back into the frequency domain. In our case, where the spectrum is a superposition of different sub-spectra (see Results), the relative intensities of different spectral contributions were calculated from the integrals over the lines of the corresponding sub-spectra.

The ^{2}H-NMR echo spectra in the intermediate exchange regime were simulated by a laboratory written Matlab program using a Liouville space formalism of the exchange process. For the powder integration over the polar angles (Eq. 3), optimized angle sets with 3,554 angles were used [78–80]. Besides the common quadrupolar fit parameters Q_{zz} (strength of the quadrupolar interaction) and η (asymmetry parameter), the jump rate k for the methyl group rotation and for the isotropic rotation during the melting process is introduced. In those cases where tunneling occurs, the spectra were simulated with a laboratory written Matlab program described elsewhere [40, 61].

3 Results and Discussions

In the following the results on these two new classes of stabile, catalytic active nanomaterials are presented. This presentation is divided into three sections. The first section presents results of a ^{2}H-solid state NMR characterization of two well defined ruthenium-polyhydrogen complexes, namely a pure hydride and a pure dihydrogen complex. These experiments identify the quadrupolar coupling of hydride type, dihydrogen type and ligand bound deuterons and create the relation between the ^{2}H-quadrupolar interaction as the relevant NMR parameter in ^{2}H-solid state NMR spectroscopy and the chemical binding situation in the complex. They allow the identification of the different deuterium species in more complex systems. In the second section this knowledge is applied to the study of ruthenium-nanoparticles interacting with hydrogen and deuterium gas. The third section then presents first results on the immobilization of the ruthenium complexes on solid silica supports.

3.1 Study of a Ruthenium-hydride and a Ruthenium-dihydrogen complex

Tp * RuD(THT)$_2$ (in the following abbreviated as **Ru-D**) is a stable hydride type ruthenium complex. It contains two THT ligands and one Tp * ligand.

***trans*-[Ru(D$_2$)Cl(dppe)$_2$]PF$_6$** (in the following abbreviated as **Ru-D$_2$**) is a stable dihydrogen type complex, which was synthesized by Morris and coworkers [81]. To the best of our knowledge this is the only dihydrogen type complex where a complete immobilization of the dihydrogen ligand down to pure coherent tunneling with a slow tunnel frequency of ca. 22 kHz can be observed.

Figure 2 compares the experimental ^{2}H-solid-echo-NMR spectra and the simulated ^{2}H-FID-NMR spectra of the **Ru-D** and the **Ru-D$_2$** complex. The set of spectra in (a) reveals temperature dependent line shapes. From their simulations three components are revealed, namely a broad Pake line with $Q_{zz} = 120$ kHz, a narrow Pake doublet with $Q_{zz} = 70$ kHz and at higher temperatures a narrow central line, which is close to a Lorentzian. The $Q_{zz} = 120$ kHz line can be attributed to –C-D groups in the organic ligands, which are results of an isotope scrambling, i.e., an H/D exchange with hydrogen positions from the organic ligands in the course of the synthesis. The central signal component which appears at higher temperatures, is also mainly attributed to –CD ligands, which in this case exhibit highly mobility. Below 170 K all mobility in the complex is frozen. The strong Pake signal with $Q_{zz} = 70$ kHz is attributed to the Ru-D hydride.

In contrast, the **Ru-D$_2$** spectra (b) contain only the signals of the two dihydrogen type deuterons with $Q_{zz} = 80$ kHz when the dihydrogen rotation is frozen and $Q_{zz} = 40$–50 kHz in the high temperature ($T > 30$ K) limit with a fast dihydrogen exchange. Since no signal of –C-D groups is visible this complex can be produced without isotope scrambling.

As mentioned above in most dihydrogen complexes the rotational barrier is so low that the hydrogens are always in the fast exchange limit. Thus we can take the value of $Q_{zz} = 40$–50 kHz as the typical value of quadrupolar couplings of dihydrogen type binding, in contrast to the value of $Q_{zz} = 70$ kHz, which is typical for hydride type binding. It follows that the quadrupolar interaction indeed is a sensitive sensor of the hydrogen binding state to a transition metal.

3.2 Study of Ruthenium-nanoparticles

Figure 3 shows the results of the ^{1}H gas phase NMR (left panel) and ^{2}H-solid state NMR experiments (right panel) on the HDA nanoparticles. The gas phase NMR study shows the production of HD from the reaction of adsorbed H with gaseous D$_2$ in a glass-sealed NMR tube. The nanoparticles are placed at the bottom of the tube well below the sensitive region of the NMR coil. The control spectrum of the

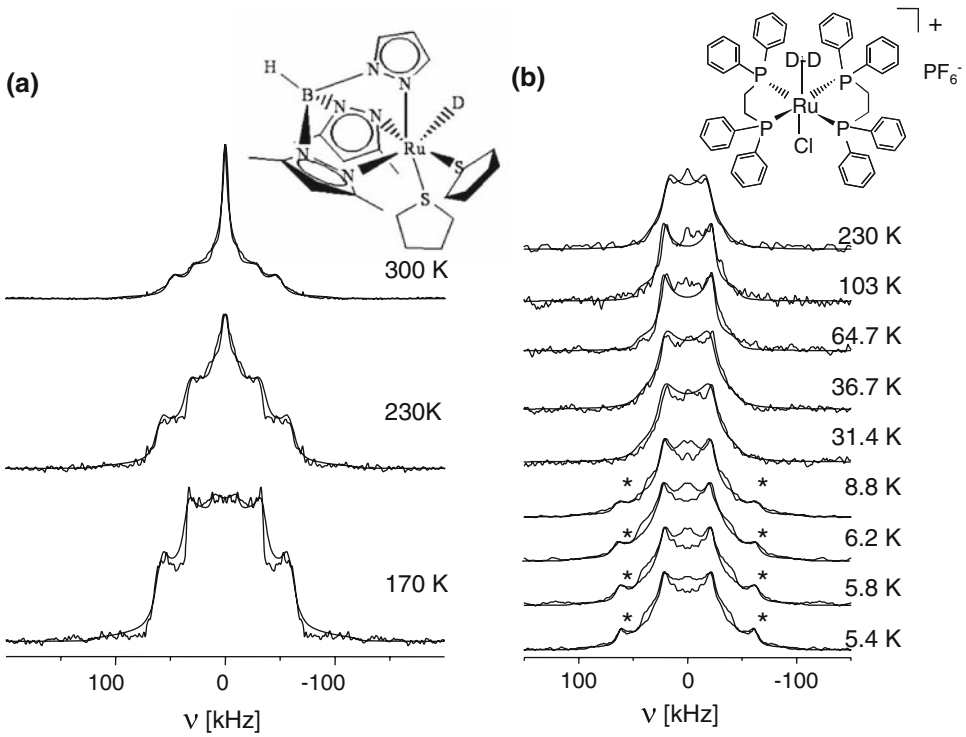

Fig. 2 ^{2}H-Solid-echo-NMR spectra (experiment and simulation) of the ruthenium–hydride complex Tp * RuD(THT)$_2$ (**a**) and the ruthenium-dihydrogen complex *trans*-[Ru(D$_2$)Cl(dppe)$_2$]PF$_6$ (**b**, adapted from Ref. [82]). While in the hydride type, sample (**a**), all dynamics is caused by ligand motions, which are frozen below 170 K, the dihydrogen type ligands can exchange classically above 10 K and by quantum mechanical tunneling below 10 K. The tunneling is visible as extra peaks in the low temperature spectra marked by asterisks

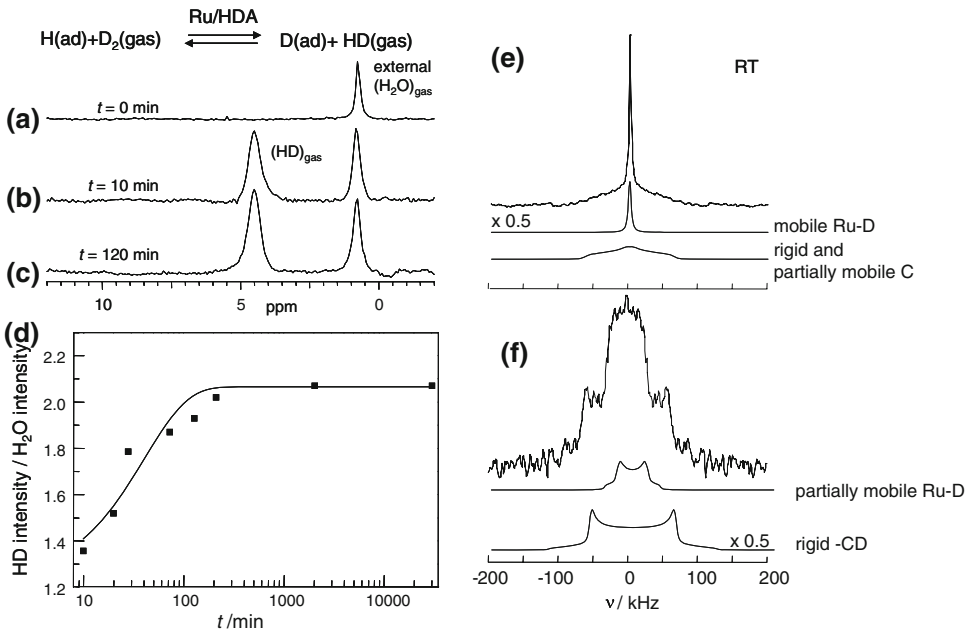

Fig. 3 11.4 T Gas phase and 7 T solid state NMR study of Ru-HAD nanoparticles (adapted from Ref. [63], see text)

evacuated NMR tube with the solid catalyst at the bottom reveals only a signal at 0.77 ppm from gaseous H_2O molecules outside the tube (Fig. 3a). In principal it is possible to remove this signal by flushing dry gaseous nitrogen through the probe; however, we preferred to employ this signal as an external intensity standard.

After exposure to D_2 during 10 min (Fig. 3b) a new peak with a line width of ca. 200 Hz arises at 4.5 ppm, which is typical for gaseous HD, showing the presence of an exchange reaction between the hydrogen adsorbed on the surface and the gaseous deuterium

$$H_{ads} + D_2 \rightleftarrows D_{ads} + HD.$$

The intensity of this peak grows further in the course of the reaction. Figure 3c shows the spectrum after a D_2 exposure of 120 min. Figure 3d displays a semi-logarithmic plot of the evolution of the HD concentration as a function of time. The solid line corresponds to a first order kinetics with exponential time dependence. The right panel of Fig. 3 shows the solid state 45.7 MHz ^{2}H-NMR spectra of a static sample of Ru/HDA particles after H/D exchange performed in the solid state. Figure 3e shows the spectrum measured at room temperature. The line shape analysis reveals two principal components: a very narrow line attributed to mobile surface Ru-D, characterized by $Q_{zz} < 1$ kHz; and a broad component which is attributed to a superposition of the spectra of immobilized and partially mobile CD groups, resulting from deuteration of the HDA ligands. Figure 3f shows the spectrum of the same sample measured at 200 K. The line shape analysis reveals partially mobile surface Ru-D, characterized by $Q_{zz} = 50$ kHz, $\eta = 0.3$ and rigid CD, characterized by $Q_{zz} = 120$ kHz, $\eta = 0.02$. The spectra of Fig. 3 provided the first detection of reactive deuterium bound to metal nanoparticles.

3.3 Immobilization of Catalysts on the Silica Support

An important step in the grafting of a catalyst on a silica surface is the spectroscopic observation of the surface species. This can be favorably done by employing a combination of ^{29}Si-, ^{13}C- and ^{31}P-CP-MAS solid state NMR, since the spectra of these nuclei are sensitive monitors of the silica surface and the reactants [12, 83–90].

The structural changes of the silica surface during processes of modification with APTES and immobilization of the ruthenium catalyst are visible in Si CP-MAS NMR spectra [29] (see Fig. 4). The Si-spectrum of the unmodified mesoporous silica material [29] (not shown) contains only three resonance peaks at −92.4, −102.4 and −112.1 ppm. They are assigned to the Q_n-type silica atoms. The Q_2- and Q_3-groups are silanol groups on the surface. While in pure silica only Q_n-groups are visible, the spectrum of APTES-modified silica displays additional lines at −59.2 and −67.1 ppm corresponding to the various T_n-groups coming from silica atoms in APTES (Fig. 4).

The appearance of the T_n-groups shows the successful functionalization of the silica surface and confirms reaction of free surface silanol groups with ethoxysilane groups from APTES. This result is corroborated by the increase in intensity of the Q_4 groups. The grafting of Ru-catalyst causes changes in the lines attributed to T_2- and Q_3-groups. One can observe the higher intensities of Q_3- and T_2-groups and the additional appearance of a T_1 signal at −55.9 ppm. These changes are strong indications for

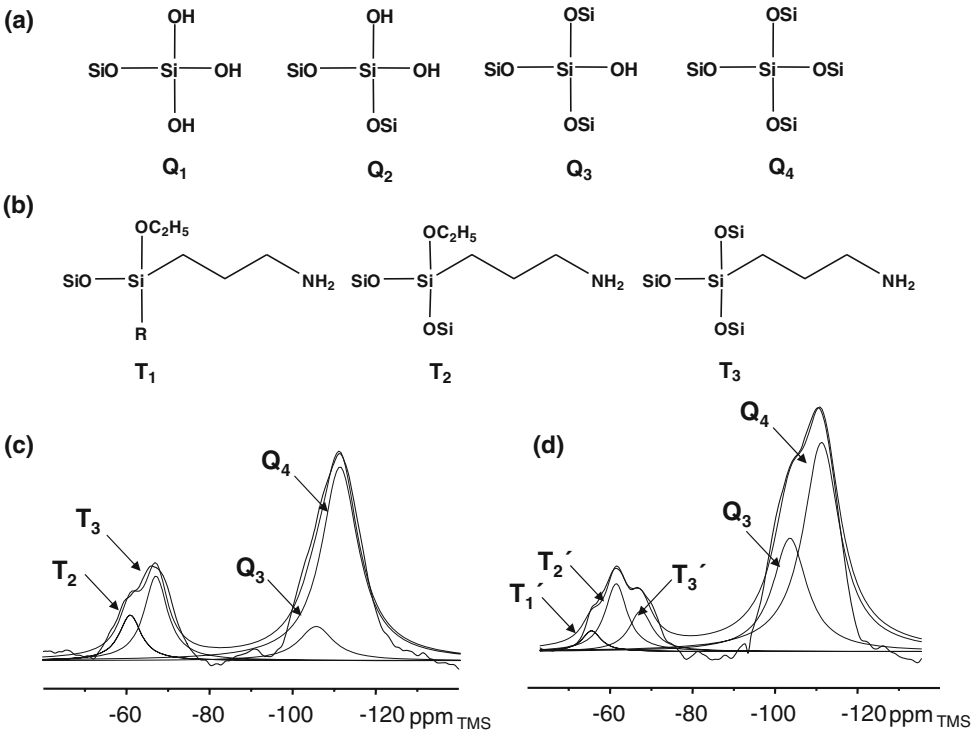

Fig. 4 (**a**, **b**) Schemes of the different types of silica atoms in the unmodified (Q_n) and modified (T_n) silica materials; (**c**) ^{29}Si CP-MAS NMR of silica SBA-3 material functionalized with APTES; (**d**) ^{29}Si CP-MAS NMR of the ruthenium catalyst immobilized on the functionalized silica surface

additional side reactions occurring due to the activity of the ruthenium catalyst.

Further insight into the successful modification of the surface and the grafting of the catalyst is gained by ^{13}C CP/MAS NMR. In the ^{13}C CP/MAS spectrum of the modified surface (Fig. 5a) one can observe signals stemming from the alkyl chain of APTES (8.6, 27.2, 42.9 ppm) and additionally two peaks of ethoxy groups (16.1 and 58.6 ppm). The presence of signals from ethoxy groups ($-OC_2H_5$) corroborates the result of the ^{29}Si CP/MAS spectra of the formation of T_1- and T_2-groups in addition to the T_3-groups, where all ethoxysilane groups have reacted with the surface.

After grafting of the ruthenium catalyst, spectra (Fig. 5b), an additional signal at 138.6 ppm appears in the

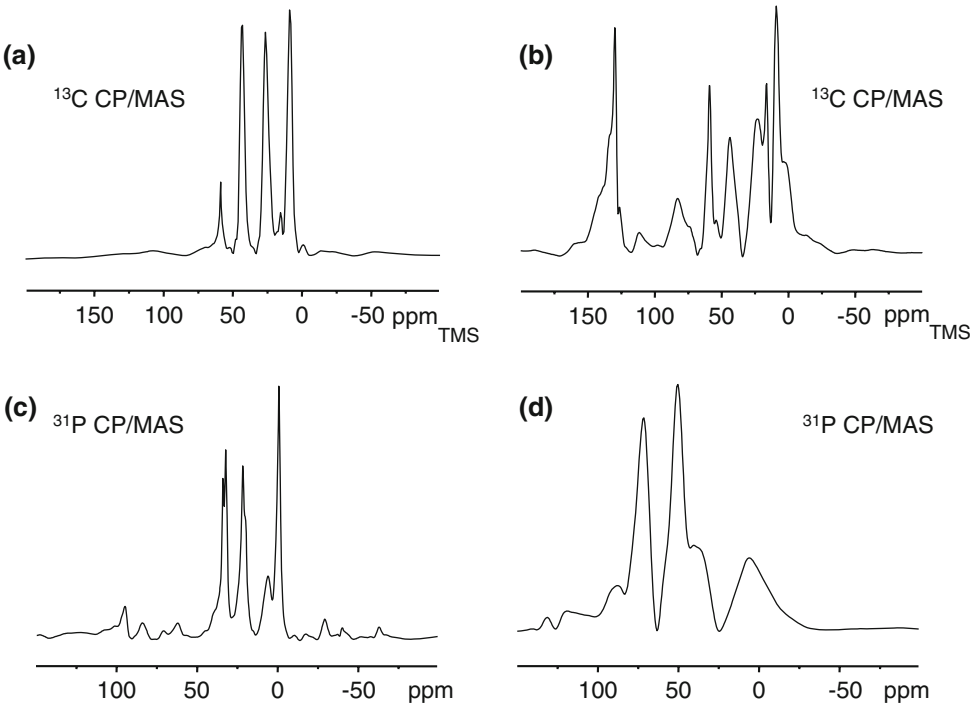

Fig. 5 ^{13}C CP/MAS of (**a**) SBA-3 modified with APTES; (**b**) ruthenium catalyst immobilized on the functionalized silica surface; ^{31}P CP/MAS of (**c**) "neat" catalyst $RuHCl(CO)(PPh_3)$; and (**d**) $RuHCl(CO)(PPh_3)$ immobilized on the silica surface

Table 1 Characteristic nitrogen adsorption data from the neat SBA-3 silica, the SBA-3 modified with APTES and the SBA-3 modified with APTES and grafted with the catalyst

	SBA-3	SBA-3 + APTES	SBA-3 + APTES + Ru
Surface (m2/g)	591	421	382
Pore diameter (nm)	3.86	–	–

The characteristic surface is clearly reduced by these steps, showing the success of the reactions. The pore diameter is given only for the neat silica, since the BJH radius becomes unreliable for small pore diameters

spectrum. This line is assigned to the phenyl group from triphosphine ligands of ruthenium catalyst.

The ^{31}P CP/MAS NMR spectra of the neat Ru-complex and the Ru-complex immobilized on the surface (Fig. 5c, d) are additional spectroscopic markers for the successful grafting. During the process of grafting the catalyst, one of the triphenylphosphine ligands is exchanged with the amine group from the APTES. In case of the "neat" Ru-complex we can observe three peaks attributed to the three PPh_3 ligands, while in the case of immobilized catalyst we have only two signals, what indicates the coordination of the amine group to the Ru atom. Thus the ^{31}P CP/MAS spectra do indeed confirm the immobilization of the ruthenium catalyst on the modified mesoporous silica surface (Table 1).

In future experiments we can now start to study the reactions of hydrogen or deuterium with these immobilized ruthenium catalysts.

4 Summary and Conclusion

As is shown above ^{2}H-solid state NMR techniques indeed provide the means for a deep characterization of the behavior of hydrogen in the coordination sphere of a transition metal or on a metal surface and can thus give new and interesting insights into basic catalytic mechanisms. Employing ^{2}H-solid state NMR spectroscopy it is possible to identify the signals of hydride type and dihydrogen type ligands bound to a metal and analyze their dynamics. This knowledge enables us to analyze the spectra of deuterium interacting with metal nanoparticles and reveal the deuterium bound to the surface. Studying the same nanoparticles with gas phase NMR gives further insight into the state of the hydrogen on the surface. As an example from the hydrogen/deuterium scrambling and the size of the quadrupolar interaction it is evident that the hydrogen is bound as a mobile hydride. Further insight into the catalytic processes is gained by gas phase NMR spectroscopy, which the kinetics of the catalytic reactions.

Finally we have shared first knowledge about or studies of the immobilization of ruthenium catalysts on silica surfaces. Employing a combination of ^{29}Si-, ^{13}C- and ^{31}P-solid state NMR, we could demonstrate the successful grafting of the catalyst on the surface. The interaction of these immobilized catalysts with hydrogen and deuterium and their application in hydrogenation reactions will be studied in the future.

Acknowledgment Financial support by the Deutsche Forschungsgemeinschaft under research grant Bu-911-12-1 is gratefully acknowledged.

References

1. Beck JS, Vartuli JC, Roth WJ, Leonowicz ME, Kresge CT, Schmitt KD, Chu CT-W, Olson DH, Sheppard EW, McCullen SB, Higgins JB, Schlenker JL (1992) J Am Chem Soc 114:10834
2. Sayari A, Hamoudi S (2001) Chem Mater 13:3151–3168
3. Linssen T, Cassiers K, Cool P, Vansant E (2003) Adv Colloid Interface Sci 103:121
4. Selvam P, Bhatia SK, Sonwane CG (2001) Ind Eng Chem Res 40:3237
5. Schreiber A, Ketelsen I, Findenegg GH (2001) Phys Chem Chem Phys 3:1185
6. Schüth F, Schmidt W (2002) Adv Eng Mater 4:269–279
7. Anwander R, Nagl I, Widenmayer M, Engelhardt G, Groeger O, Palm C, Röser T (2000) J Phys Chem B 104:3532
8. Whilton NT, Berton B, Bronstein L, Hentze H-P, Antonietti M (1999) Adv Mater 11:1014
9. Vinu A, Hossain KZ, Ariga K (2005) J Nanosci Nanotechnol 5:347–371
10. Morey MS, Davidson A, Stucky GD (1998) J Porous Mater 5:195–204
11. Chen HT, Huh S, Wiench JW, Pruski M, Lin VSY (2005) Abstr Pap Am Chem Soc 229:U983
12. Chen HT, Huh S, Wiench JW, Pruski M, Lin VSY (2005) J Am Chem Soc 127:13305–13311
13. Wang XG, Lin KSK, Chan JCC, Cheng SF (2005) J Phys Chem B 109:1763–1769
14. Vinu A, Miyahara M, Ariga K (2006) J Nanosci Nanotechnol 6:1510–1532
15. Aksnes DW, Gjerdaker L (1999) J Mol Struct 27
16. Courivaud F, Hansen EW, Kolboe S, Karlsson A, Stöcker M (2000) Microporous Mesoporous Mater 37:223
17. Jobic H (1999) Phys Chem Chem Phys 1:525
18. Ladizhansky V, Hodes G, Vega S (2000) J Phys Chem B 104:1939
19. Mel'nichenko YB, Schüller J, Richert R, Ewen B, Loong C-K (1995) J Chem Phys 103:2016
20. Gjerdaker L, Sorland GH, Aknes DW (1999) Microporous Mesoporous Mater 32:305
21. Hansen EW, Schmidt R, Stöcker M, Akporiaye D (1995) Microporous Mater 5:143
22. Gedat E, Schreiber A, Albrecht J, Shenderovich I, Findenegg G, Limbach H-H, Buntkowsky G (2002) J Phys Chem B 106:1977
23. Valiullin R, Naumov S, Galvosas P, Kärger J, Woo H-J, Porcheron F, Monson PA (2006) Nature 443:965
24. Buntkowsky G, Breitzke H, Adamczyk A, Roelofs F, Emmler T, Gedat E, Grünberg B, Xu Y, Limbach HH, Shenderovich I, Vyalikh A, Findenegg GH (2007) Phys Chem Chem Phys 9(35):4843–4853

25. Niu SQ, Thomson LM, Hall MB (1998) J Am Chem Soc 121:4000
26. Cucullu ME, Nolan SP, Belderrain TR, Grubbs RH (1998) Organometallics 17:1299
27. Lough AJ, Morris RH, Ricciuto L, Schleis T (1998) Inorg Chim Acta 270:238
28. Esteruelas MA, Oro LA (1998) Chem Rev 98:577
29. Matthes J, Grundemann S, Toner A, Guari Y, Donnadieu B, Spandl J, Sabo-Etienne S, Clot E, Limbach HH, Chaudret B (2004) Organometallics 23:1424–1433
30. Maseras F, Lledos A, Clot E, Eisenstein O (2000) Chem Rev 100:601–636
31. Macchioni A (2005) Chem Rev 105:2039–2073
32. Lachaize S, Essalah W, Montiel-Palma V, Vendier L, Chaudret B, Barthelat JC, Sabo-Etienne S (2005) Organometallics 24:2935–2943
33. Aebischer N, Frey U, Merbach AE (1998) Chem Comm 2303
34. Albertin G, Antoniutti S, Garciafontan S, Carballo R, Padoan F (1998) J Chem Soc Dalton trans 2071
35. Alkorta I, Rozas I, Elguero J (1998) Chem Soc Rev 27:163
36. Bakhmutov VI (1998) Inorg Chem 37:279
37. Bartucz TY, Golombek A, Lough AJ, Maltby PA, Morris RH, Ramachandran R, Schlaf M (1998) Inorg Chem 37:1555
38. Basallote MG, Duran J, Fernandez-Trujillo MJ, Manez MA (1998) J Chem Soc Dalton Trans 2205
39. Bohanna C, Callejas B, Edwards AJ, Esteruelas MA, Lahoz FJ, Oro LA, Ruiz N, Valero C (1998) Organometallics 17:373
40. Buntkowsky G, Limbach H-H, Wehrmann F, Sack I, Vieth HM, Morris RH (1997) J Phys Chem A 101:4679
41. Chaudret B (1998) Coord Chem Rev 180:381
42. Cooper AC, Caulton KG (1998) Inorg Chem 37:5938
43. Crabtree RH (1998) J Organomet Chem 557:111
44. Gelabert R, Moreno M, Lluch JM, Lledos A (1998) J Am Chem Soc 120:8168
45. Gründemann S, Limbach H-H, Rodriguez V, Donnadieu B, Sabo-Etienne S, Chaudret B (1998) Ber Bunsen Phys Chem 102:344
46. Hasegawa T, Li ZW, Taube H (1998) Chem Lett 7
47. Limbach H-H, Ulrich S, Gründemann S, Buntkowsky G, Sabo-Etienne S, Chaudret B, Kubas GJ, Eckert J (1998) J Am Chem Soc 120:7929
48. Macfarlane KS, Thorburn IS, Cyr PW, Chau D, Rettig SJ, James BR (1998) Inorg Chim Acta 270:130
49. Ng WS, Jia GC, Huang MY, Lau CP, Wong KY, Wen LB (1998) Organometallics 17:4556
50. Popelier PLA (1998) J Phys Chem A 102:1873
51. Sabo-Etienne S, Chaudret B (1998) Chem Rev 98:2077
52. Stahl SS, Labinger JA, Bercaw JE (1998) Inorg Chem 37:2422
53. Kubas GJ, Ryan RR, Swanson BI, Vergamini PJ, Wasserman HJ (1984) J Am Chem Soc 116:451
54. Kubas GJ (1988) J Acc Chem Res 21:120
55. Jessop PG, Morris RH (1992) Coord Chem Rev 121:155
56. Heinekey DM, Oldham WJ (1993) J Chem Rev 93:913
57. Luther TA, Heinekey DM (1998) Inorg Chem 37:127
58. Toupadakis A, Kubas GJ, King WA, Scott LB, Huhmann-Vincent J (1998) Organometallics 17:5315
59. Maltby PA, Steinbeck M, Lough AJ, Morris RH, Klooster WT, Koetzle TF, Srivastava RC (1996) J Am Chem Soc 118:5396
60. Buntkowsky G, Limbach HH (2006) In: Hynes JP, Klinman JP, Limbach HH, Schowen RL (eds) Hydrogen-transfer reactions, vol 2. Wiley-VCH, Weinheim, pp 639–682
61. Buntkowsky G, Limbach HH (2006) J Low Temp Phys 143: 55–114
62. Wehrmann F, Albrecht J, Gedat E, Kubas GJ, Limbach HH, Buntkowsky G (2002) J Phys Chem A 106:2855
63. Pery T, Pelzer K, Buntkowsky G, Philippot K, Limbach HH, Chaudret B (2005) Chem Phys Chem 6:605
64. Garcia-Anton J, Rosa Axet M, Jansat S, Philippot K, Chaudret B, Pery T, Buntkowsky G, Limbach HH (2008) Angew Chem Int Edit accepted for publication
65. Matthes J, Pery T, Gründemann S, Buntkowsky G, Sabo-Etienne S, Limbach HH, Chaudret B (2004) J Am Chem Soc 126:8366
66. Buntkowsky G, Walaszek B, Adamczyk A, Xu Y, Limbach H-H, Chaudret B (2006) Phys Chem Chem Phys 8:1929–1935
67. Huo QS, Margolese DI, Stucky GD (1996) Chem Mater 8: 1147–1160
68. Zhao DY, Huo QS, Feng JL, Chmelka BF, Stucky GD (1998) J Am Chem Soc 120:6024–6036
69. Dai L, Wang T, Bu L, Chen G (2001) Colloid Surf A 181: 151–157
70. Ahmad N, Levison JJ, Robinson SD, Uttley MF (1990) Inorg Synth 28:81–83
71. Joseph T, Deshpande SS, Halligudi SB, Vinu A, Ernst S, Hartmann M (2003) J Mol Catal A: Chem 206:13–21
72. Pan C, Pelzer K, Philippot K, Chaudret B, Dassenoy F, Lecante P, Casanove MJ (2001) J Am Chem Soc 123:7584
73. Slichter CP (1990) Principles of magnetic resonance, 3rd edn. Springer Verlag, Berlin Heidelberg New York
74. Schmidt-Rohr K, Spiess HW (1994) Multidimensional solid state NMR and polymers. Academic Press, London
75. Detken A, Zimmermann H (1998) J Chem Phys 108:5845
76. Mehring M (1983) High resolution NMR spectroscopy in solids. Springer Verlag, Berlin Heidelberg New York
77. Schmidt-Rohr K, Nanz D, Emsley L, Pines A (1994) J Phys Chem 98:6668
78. Zaremba SK (1966) Ann Mat Pure Appl 4:293
79. Conroy H (1967) J Chem Phys 47:5307
80. Cheng VB, Suzukawa HH, Wolfsberg M (1973) J Chem Phys 59:3992
81. Chin B, Lough AJ, Morris RH, Schweitzer CT, D'Agostino C (1994) Inorg Chem 33:6278
82. Wehrmann F, Fong T, Morris RH, Limbach H-H, Buntkowsky G (1999) Phys Chem Chem Phys 1:4033
83. Bluemel J (1995) Ber Bunsen Phys Chem 99:1343–1346
84. Merckle C, Bluemel J (2001) Chem Mater 13:3617–3623
85. Merckle C, Haubrich S, Bluemel J (2001) J Organomet Chem 627:44–54
86. Merckle C, Bluemel J (2005) Top Catal 34:5–15
87. Bluemel J (2006) Nachr Chem 54:632–638
88. Trebosc J, Wiench JW, Huh S, Lin VSY, Pruski M (2005) J Am Chem Soc 127:3057–3068
89. Huh S, Chen HT, Wiench JW, Pruski M, Lin VSY (2005) Angew Chem Int Edit 44:1826–1830
90. Trebosc J, Wiench JW, Huh S, Lin VSY, Pruski M (2005) J Am Chem Soc 127:7587–7593